

LaPro-DTA: Latent Dual-View Drug Representations and Salient Protein Feature Extraction for Generalizable Drug–Target Affinity Prediction

Zihan Dun¹, Liuyi Xu¹, An-Yang Lu¹, Shuang Li², Yining Qian^{3*}

¹College of Information Science and Engineering, Northeastern University, Shenyang 110819, China

²School of Artificial Intelligence, Beihang University, Beijing 100000, China

³School of Computer Science and Engineering, Northeastern University, Shenyang 110819, China
dunzihan@stumail.yzu.edu.cn, {xuliuyi, luanyang}@mails.neu.edu.cn, shuangliai@buaa.edu.cn, qianyingning@126.com

Abstract

Drug–target affinity prediction is pivotal for accelerating drug discovery, yet existing methods suffer from significant performance degradation in realistic cold-start scenarios (unseen drugs/targets/pairs), primarily driven by overfitting to training instances and information loss from irrelevant target sequences. In this paper, we propose LaPro-DTA, a framework designed to achieve robust and generalizable DTA prediction. To tackle overfitting, we devise a latent dual-view drug representation mechanism. It synergizes an instance-level view to capture fine-grained substructures with stochastic perturbation and a distribution-level view to distill generalized chemical scaffolds via semantic remapping, thereby enforcing the model to learn transferable structural rules rather than memorizing specific samples. To mitigate information loss, we introduce a salient protein feature extraction strategy using pattern-aware top- k pooling, which effectively filters background noise and isolates high-response bioactive regions. Furthermore, a cross-view multi-head attention mechanism fuses these purified features to model comprehensive interactions. Extensive experiments on benchmark datasets demonstrate that LaPro-DTA significantly outperforms state-of-the-art methods, achieving an 8% MSE reduction on the Davis dataset in the challenging unseen-drug setting, while offering interpretable insights into binding mechanisms.

1 Introduction

Drug–target affinity (DTA) measures the binding strength between drug molecules and target proteins, serving as a cornerstone in virtual screening and lead optimization [Chen *et al.*, 2025; Li *et al.*, 2023]. While traditional biochemical assays provide precise measurements, they are often prohibitively expensive and time-consuming, limiting their scalability for large-scale chemical space exploration [Prasad and Mailankody, 2017]. Consequently, developing efficient data-

driven computational methods has become indispensable for accelerating modern drug discovery.

The complexity of molecular interactions has driven a paradigm shift from classical machine learning to deep learning architectures [Kim *et al.*, 2021; Watanabe *et al.*, 2021]. Early computational approaches mainly employed machine learning techniques for DTA prediction [Ain *et al.*, 2015; He *et al.*, 2017]. With the adoption of deep learning, DTA prediction methods have increasingly moved toward end-to-end models that learn task-specific representations directly from raw input data [Yang *et al.*, 2024; Li *et al.*, 2020; Zhao *et al.*, 2020; Fang *et al.*, 2023]. DeepDTA [Öztürk *et al.*, 2018] used CNNs to model local patterns in protein and drug sequences, while GraphDTA [Nguyen *et al.*, 2021] adopted graph neural networks to represent molecular structures. To improve the accuracy of DTA prediction, recent works have been proposed to investigate the capture of more effective drug features by incorporating multi-task learning methods with reconstruction tasks or using multi-model approaches [Li *et al.*, 2021; Zhang *et al.*, 2024]. For instance, [Qian *et al.*, 2025; Shah *et al.*, 2025] have been proposed to enhance feature representation via reconstruction, and DMFF-DTA [He *et al.*, 2025] has been proposed to investigate the integration of sequence and graph structural information from both drugs and target proteins to improve affinity prediction performance. Collectively, these methods have established strong baselines on standard benchmarks.

However, a critical gap remains: their success is largely confined to random split settings, where test data follows the same distribution as training data. In realistic cold-start scenarios—where models must predict affinity for unseen drugs or targets—existing state-of-the-art methods suffer from significant performance degradation [Huang *et al.*, 2025; Choppara and Lokesh, 2025]. This generalization gap suggests that current methods often rely on memorizing training instances rather than learning the transferable chemical rules governing molecular interactions. We attribute this failure to two fundamental bottlenecks in current DTA representation learning: **(1) Overfitting to instances:** Existing approaches typically treat drug–target pairs as isolated labels. Lacking a mechanism to capture generalizable Structure-Activity Relationships (SAR) [Bemis and Murcko, 1996], models tend to memorize specific training samples and their syntactic shortcuts rather than learning transferable chemical scaffolds.

*Corresponding author.

This overfitting is often exacerbated by auxiliary reconstruction tasks, which can introduce optimization conflicts distinct from the primary affinity objective [Shah *et al.*, 2025]. **(2) Information loss from irrelevant target sequences:** Drug-target binding is inherently localized to specific active sites, whereas most methods compress the full-length target sequence into a single global representation. This mismatch causes salient binding signals to be diluted by the vast non-functional protein background [Zhao *et al.*, 2019]. Without a mechanism to prioritize high-response features, models tend to average out critical local patterns with irrelevant protein segments, which severely compromises their capability to generalize to unseen targets [Huang *et al.*, 2021].

To bridge this gap, we propose LaPro-DTA: **Latent dual-view drug representations and salient Protein feature extraction**, a novel framework designed for robust and generalizable DTA prediction. We devise a dual-view representation learning mechanism for drugs and a salient feature extraction strategy for proteins, respectively. Furthermore, a cross-view multi-head attention mechanism facilitates deep interaction between these purified representations for comprehensive affinity modeling. Our main contributions are:

- We propose a latent dual-view drug representation framework that synergizes an instance-level view to capture fine-grained substructures and a distribution-level view to distill generalized chemical scaffolds via semantic remapping. By incorporating a stochastic encoding strategy, we provide a mathematically grounded solution acting as implicit regularization to effectively mitigate overfitting in data-scarce cold-start scenarios.
- We develop a salient protein feature extraction strategy utilizing pattern-aware top- k pooling. This mechanism functions as a semantic filter, explicitly discarding redundancy from non-binding regions while preserving the most discriminative bio-active features. Crucially, this selective retention mitigates the loss of critical information, facilitating precise interaction modeling.
- We conduct extensive evaluations on standard benchmarks and a strictly disjoint out-of-sample test set, demonstrating that LaPro-DTA establishes new state-of-the-art performance across unseen settings and offers superior interpretability through visualized residue-level saliency analysis.

2 Methodology

As illustrated in Figure 1, LaPro-DTA comprises three core components: latent dual-view drug representation, salient protein feature extraction, and cross-view feature fusion with affinity prediction.

2.1 Problem Formulation

We formulate the DTA prediction task as a regression problem. Let $\mathcal{D} = \{d_1, d_2, \dots, d_N\}$ denote the set of drug molecules, where each drug is represented by its SMILES string [Weininger, 1988]. Similarly, let $\mathcal{T} = \{t_1, t_2, \dots, t_M\}$ denote the set of target proteins, where each target is represented by its amino acid sequence. The interactions are

provided as an affinity matrix $\mathbf{Y} \in \mathbb{R}^{N \times M}$, where y_{ij} represents the continuous binding affinity value between drug d_i and target t_j . The objective is to learn a predictive function $f : \mathcal{D} \times \mathcal{T} \rightarrow \mathbb{R}$ that accurately estimates the affinity score for a given drug-target pair. Crucially, under cold-start settings, the drug d or target t encountered at inference time is unseen during training.

2.2 Drug Representation Modeling and Latent Dual-View Mechanism

Main Idea. To mitigate **overfitting**, we introduce a latent dual-view mechanism. This design discourages the model from capturing syntactic shortcuts, shifting its focus to features governed by distributional regularities.

Instance-Level View. We define a shared encoder \mathcal{E} to extract latent representations of drugs. Specifically, \mathcal{E} first employs a GatedCNN block [Dauphin *et al.*, 2017] to capture local substructural features from the input drug embedding $\mathbf{X}_d \in \mathbb{R}^{L_d \times d_e^d}$. This block consists of three stacked convolutional layers where information flow is controlled by the element-wise product of a linear convolutional feature map and a sigmoid-activated gate. Subsequently, the encoder projects these features into latent distribution parameters: the mean $\boldsymbol{\mu}_{ins} \in \mathbb{R}^{d_z}$ and the log-variance $\mathbf{h}_{var} \in \mathbb{R}^{d_z}$.

To enhance representation robustness, we propose a **stochastic encoding strategy (SES)**. The instance-level sampling process is defined as:

$$\mathbf{z}_{ins} = \boldsymbol{\mu}_{ins} + \boldsymbol{\epsilon} \odot \boldsymbol{\sigma}_{ins}, \quad \boldsymbol{\epsilon} \sim \mathcal{N}(\mathbf{0}, \mathbf{I}) \quad (1)$$

where $\boldsymbol{\sigma}_{ins} = \lambda \cdot \exp\left(\frac{1}{2}\text{ReLU}(\mathbf{h}_{var})\right)$. Here, we enforce a hard architectural constraint using a ReLU activation to ensure the standard deviation has a lower bound λ , preventing the latent space from collapsing into deterministic points. Theoretically, this stochastic sampling under the lower-bound constraint acts as an implicit Tikhonov regularization [Bishop, 1995]. To demonstrate this, let $F : \mathbb{R}^{d_z} \rightarrow \mathbb{R}$ denote the downstream affinity prediction function. To isolate the regularization effect, we temporarily focus on the instance-level view \mathbf{z}_{ins} by treating other views and target features as constants. By applying a first-order Taylor expansion to F around $\boldsymbol{\mu}_{ins}$, the expected loss under perturbation $\boldsymbol{\epsilon}$ can be approximated as:

$$\begin{aligned} \mathbb{E}_{\boldsymbol{\epsilon}}[\tilde{\mathcal{L}}] &\approx \mathbb{E}_{\boldsymbol{\epsilon}} \left[(y - F(\boldsymbol{\mu}_{ins}) - \nabla F^\top(\boldsymbol{\sigma}_{ins} \odot \boldsymbol{\epsilon}))^2 \right] \\ &= \mathcal{L}_{MSE} + \sum_i (\sigma_{ins,i} \cdot \partial_{z_i} F)^2 \\ &\geq \mathcal{L}_{MSE} + \lambda^2 \|\nabla F(\boldsymbol{\mu}_{ins})\|_2^2 \end{aligned} \quad (2)$$

where the cross-terms vanish since $\mathbb{E}[\boldsymbol{\epsilon}] = \mathbf{0}$. The constraint $\boldsymbol{\sigma}_{ins} \geq \lambda$ imposes a strict penalty on the gradient norm $\|\nabla F\|_2^2$. This effectively smoothes the decision boundaries of the prediction function, thereby preventing overfitting in data-scarce cold-start settings.

Distribution-Level View. Relying solely on instance-level representations suffers from a critical limitation: models tend to memorize specific input details, failing to learn the generalized regularities necessary for extrapolating to unseen drug scenarios. To bridge this gap, we introduce a

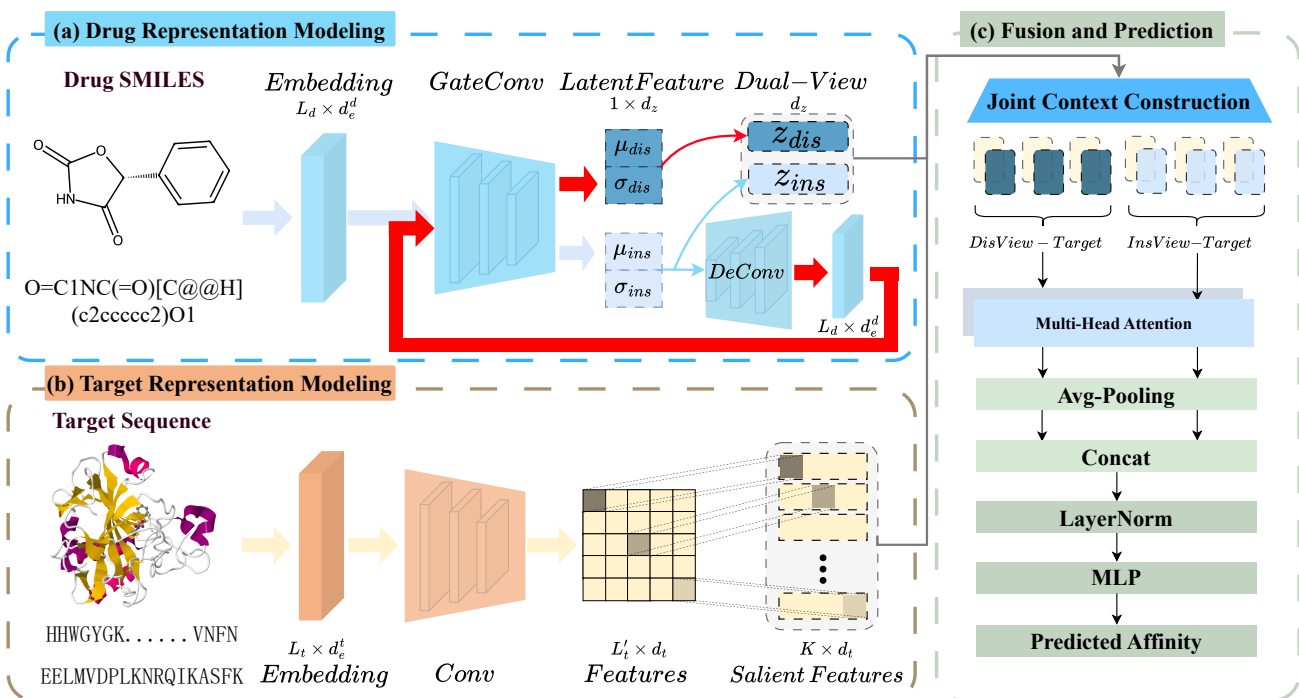


Figure 1: Overview of the LaPro-DTA architecture. (a) Drug Representation: Extracts drug features using a dual-view mechanism to capture both instance-level and distribution-level view. (b) Target Representation: Extracts target features by selectively focusing on key bioactive segments rather than the whole sequence. (c) Feature Fusion and Prediction: Aligns drug and target features to capture fine-grained interactions between them. The red line denotes the DeCNN-to-shared-encoder route that generates the distribution-level view.

distribution-level view designed to distill generalized structural regularities from the chemical space. Formally, we employ a DeCNN module [Zeiler *et al.*, 2010] to map the compressed instance latent \mathbf{z}_{ins} to an intermediate feature map $\mathbf{H}_{remap} \in \mathbb{R}^{L_d \times d_e^d}$. Distinct from autoencoders that depend on token-wise reconstruction losses to memorize inputs, our approach performs a *task-driven semantic remapping*. We feed \mathbf{H}_{remap} back into the shared encoder \mathcal{E} to generate the final distribution-level representation \mathbf{z}_{dis} :

$$[\boldsymbol{\mu}_{dis}, \boldsymbol{\sigma}_{dis}] = \mathcal{E}(\mathbf{H}_{remap}) \quad (3)$$

$$\mathbf{z}_{dis} = \boldsymbol{\mu}_{dis} + \epsilon \odot \boldsymbol{\sigma}_{dis}, \quad \epsilon \sim \mathcal{N}(0, \mathbf{I}) \quad (4)$$

In this process, by eliminating the constraint of token-wise reconstruction, we decouple feature learning from the memorization of trivial input details. Instead, under the exclusive guidance of the discriminative DTA objective, the remapping process is compelled to distill only those distributional regularities that are predictively critical for drug-target interactions. This mechanism effectively filters out instance-specific noise while retaining the robust chemical scaffolds necessary for accurate affinity modeling, thereby providing a distribution-level perspective with enhanced generalization capabilities.

Dual-View Synergy. Guided by the SAR principle [Bemis and Murcko, 1996], our mechanism addresses the challenge where similar structures share bioactivities yet subtle variations alter affinity. The distribution-level view captures generalized chemical scaffolds, enabling inference on unseen en-

ties via broad structural regularities. Complementarily, the instance-level view resolves fine-grained atomic details, distinguishing specific interactions within local substructures. Integrating these perspectives balances the extrapolation capability needed for cold-start scenarios with the discrimination precision required for accurate prediction.

2.3 Salient Target Features Extraction with Pattern-Aware Top-K Pooling

Main Idea. To mitigate **information loss** caused by global compression, we propose a salient feature extraction strategy that acts as a selective filter. Using top- k pooling, this mechanism prioritizes high-activation features, explicitly retaining only the most discriminative local patterns while filtering out redundancy. We use stacked CNNs to extract local representations from the target protein embedding $\mathbf{X}_t \in \mathbb{R}^{L_t \times d_e}$. With this architecture, the convolutional filters act as specific feature detectors, capturing contextualized local structures (e.g., motifs) into feature channels.

Pattern-Aware Top-K Pooling. [Kalchbrenner *et al.*, 2014] demonstrated the effectiveness of k -max pooling in capturing the most informative sequence elements. Drawing on this, we adapt this mechanism to construct compact **salient features**. To retain high-value information, we adopt a high-activation priority strategy. This design explicitly preserves dominant residue sets, ensuring that the downstream attention mechanism focuses on the most reactive biochemical patterns. Formally, let $\mathbf{H}_{conv} \in \mathbb{R}^{L'_t \times d_t}$ denote the convolutional feature

map, where d_t is the number of filters. We identify the K most significant activations for each channel independently:

$$\mathbf{H}_t = \text{TopK}(\mathbf{H}_{conv}, K) \quad (5)$$

This representation $\mathbf{H}_t \in \mathbb{R}^{K \times d_t}$ aggregates the top- k activations, where each entry corresponds to a critical residue within the sequence. This hyperparameter selection aligns with the sparsity assumption of binding pockets, suggesting that identifying the top few strongest activations per channel is sufficient to characterize the presence of specific biochemical motifs while suppressing redundant information. Finally, the salient features serve as the input for the fusion module. This ranking-based profile aggregates the strongest responses across all pattern detectors, robustly capturing key binding evidence. This capability is corroborated by our analysis of residue-level saliency maps in Section 3.8.

2.4 Cross-View Multi-Head Attention Fusion and Affinity Prediction

Main Idea. To leverage the dual-view drug representations and high-response protein features, we propose a cross-view multi-head attention fusion module. Unlike global pooling which causes attention degeneration, our top- k strategy preserves salient protein features, providing granular context for fine-grained interaction modeling.

Joint Context Construction. Drug vectors (\mathbf{z}_{ins} and \mathbf{z}_{dis}) are broadcasted to match the cardinality K of the protein segments (\mathbf{H}_t) and concatenated, followed by a linear projection to form context matrices $\mathbf{C}_{ins} \in \mathbb{R}^{K \times d_t}$ and $\mathbf{C}_{dis} \in \mathbb{R}^{K \times d_t}$. This design addresses two realistic scenarios: (1) instance-level detail context (\mathbf{C}_{ins}) captures precise atom-level details for identifying trained or similar drugs; (2) distribution-level representation context (\mathbf{C}_{dis}) facilitates cold-start generalization by leveraging scaffold similarity to infer binding potential for unseen molecules. The drug representations $\mathbf{z}_{ins}, \mathbf{z}_{dis} \in \mathbb{R}^{d_z}$ are spatially aligned with the protein segments $\mathbf{H}_t \in \mathbb{R}^{K \times d_t}$ via broadcasting. The construction of the local context matrix \mathbf{C}_{ins} is defined as:

$$\mathbf{C}_{ins} = \phi([\mathbf{1}_K \mathbf{z}_{ins}^\top \parallel \mathbf{H}_t] \mathbf{W}_i + \mathbf{b}_i) \quad (6)$$

where $\mathbf{1}_K \in \mathbb{R}^{K \times 1}$ is a vector of ones, and \parallel denotes the concatenation along the feature dimension. Similarly, the distribution-level representation matrix \mathbf{C}_{dis} is formulated as:

$$\mathbf{C}_{dis} = \phi([\mathbf{1}_K \mathbf{z}_{dis}^\top \parallel \mathbf{H}_t] \mathbf{W}_d + \mathbf{b}_d) \quad (7)$$

In both cases, $\mathbf{W}_i, \mathbf{W}_d \in \mathbb{R}^{(d_z + d_t) \times d_t}$ are learnable projection matrices and $\phi(\cdot)$ is the non-linear activation function. **Attention Fusion and Prediction.** We employ multi-head attention where protein segments \mathbf{H}_t serve as the Query (\mathbf{Q}), while the joint contexts act as both Key (\mathbf{K}) and Value (\mathbf{V}). For the instance-level view interaction:

$$\mathbf{Q} = \mathbf{H}_t, \quad \mathbf{K} = \mathbf{V} = \mathbf{C}_{ins}, \quad \mathbf{O}_{ins} = \text{Softmax}\left(\frac{\mathbf{Q}\mathbf{K}^\top}{\sqrt{d_t}}\right) \mathbf{V} \quad (8)$$

The global output \mathbf{O}_{dis} is computed analogously. Finally, the affinity \hat{y} is predicted by aggregating the dual-view features:

$$\hat{y} = \text{MLP}(\text{LN}([\text{Mean}(\mathbf{O}_{ins}) \parallel \text{Mean}(\mathbf{O}_{dis})])) \quad (9)$$

Optimization Objective: We adopt the Mean Squared Error (MSE) as the objective function to minimize the discrepancy between the ground-truth affinity y_i and the predicted value \hat{y}_i . The loss \mathcal{L} is defined as:

$$\mathcal{L}_{MSE} = \frac{1}{N} \sum_{i=1}^N (y_i - \hat{y}_i)^2 \quad (10)$$

Dataset	Drugs	Targets	Interactions	Affinity metrics
KIBA	2,111	229	118,254	K_d, K_i and IC_{50}
Davis	68	442	30,056	K_d

Table 1: Summary of the datasets used in our experiments.

3 Experiments and Results

3.1 Datasets

We evaluate LaPro-DTA on two benchmark datasets: Davis [Davis *et al.*, 2011] and KIBA [Tang *et al.*, 2014]. Following standard protocols, the interaction values in Davis are converted into their negative logarithmic forms (pK_d). Detailed statistics are summarized in Table 1.

Settings. To rigorously assess generalization, we design two distinct experimental protocols:

Cold-Start Setting (Primary Focus). To simulate realistic drug discovery, we randomly reserve 20% of drugs and targets as unseen entities. Based on this partition, the dataset is systematically stratified into three distinct scenarios: unseen drug (test drugs \times training targets), unseen target (training drugs \times test targets), and unseen pair (both unseen). For each scenario, the interactions are split equally into validation and testing sets, ensuring that test entities remain strictly unobserved during training.

Random Split Setting. Additionally, we conduct experiments under the standard random split setting (randomly dividing interactions into train/validation/test sets) to serve as a performance reference. Detailed results for this setting are provided in Table S2 of the Supplementary Material.

3.2 Experimental Details

Hyperparameter Settings. LaPro-DTA is implemented in PyTorch 2.0 and trained on a single NVIDIA RTX 3090 GPU. The model is optimized using Adam with a learning rate of 5×10^{-4} and a batch size of 256. To mitigate overfitting, we employ an early stopping strategy with a patience of 20 epochs (maximum 100 epochs). The Drug Encoder employs a 3-block Gated CNN (kernel size 4) with a latent dimension of $d = 96$. The Protein Encoder consists of a 3-layer CNN followed by top- k pooling ($k = 4$). For the distribution-level view, a DeCNN restores feature maps processed by a Re-encoder that shares weights with the Drug Encoder. Finally, the fusion module utilizes multi-head attention ($h = 4$) followed by a prediction MLP. Comprehensive hyperparameter details are provided in the Supplementary Material.

Evaluation Metrics. Consistent with [He *et al.*, 2025], performance is evaluated using four standard metrics: Mean Absolute Error (MAE) and Mean Squared Error (MSE) quantify the deviation between predicted and actual affinities. The

Model	Davis				KIBA			
	MSE (std) ↓	MAE (std) ↓	CI (std) ↑	r_m^2 (std) ↑	MSE (std) ↓	MAE (std) ↓	CI (std) ↑	r_m^2 (std) ↑
<i>Setting: Unseen Drug</i>								
DeepDTA (2018)	0.745 (0.008)	0.704 (0.050)	0.699 (0.045)	0.078 (0.023)	0.478 (0.007)	0.485 (0.004)	0.688 (0.006)	0.263 (0.002)
AttentionDTA (2019)	0.656 (0.004)	0.622 (0.003)	0.682 (0.010)	0.104 (0.004)	0.433 (0.041)	0.432 (0.031)	0.722 (0.025)	0.322 (0.030)
Co-VAE (2021)	0.577 (0.009)	0.523 (0.001)	0.616 (0.005)	0.128 (0.014)	0.429 (0.019)	0.459 (0.041)	0.745 (0.010)	0.334 (0.019)
GraphDTA (2021)	0.590 (0.016)	0.552 (0.014)	0.695 (0.008)	0.077 (0.010)	0.473 (0.021)	0.526 (0.020)	0.738 (0.004)	0.282 (0.032)
ColdDTA (2023)	0.613 (0.012)	0.522 (0.008)	0.716 (0.020)	0.146 (0.012)	0.427 (0.018)	0.448 (0.030)	0.722 (0.008)	0.329 (0.029)
TransVAE-DTA (2024)	0.654 (0.030)	0.559 (0.016)	0.570 (0.021)	0.030 (0.017)	0.537 (0.047)	0.501 (0.036)	0.715 (0.024)	0.201 (0.031)
PairVAE (2025)	0.566 (0.004)	0.498 (0.007)	0.730 (0.003)	0.134 (0.036)	0.469 (0.031)	0.469 (0.016)	0.727 (0.007)	0.328 (0.024)
LaPro-DTA (ours)	0.519 (0.010)	0.454 (0.009)	0.737 (0.001)	0.191 (0.028)	0.403 (0.014)	0.409 (0.014)	0.755 (0.004)	0.352 (0.024)
<i>Setting: Unseen Target</i>								
DeepDTA (2018)	0.884 (0.024)	0.711 (0.008)	0.751 (0.033)	0.183 (0.015)	0.542 (0.012)	0.498 (0.019)	0.706 (0.015)	0.365 (0.024)
AttentionDTA (2019)	0.565 (0.014)	0.560 (0.022)	0.814 (0.002)	0.450 (0.033)	0.543 (0.029)	0.493 (0.013)	0.704 (0.021)	0.349 (0.023)
Co-VAE (2021)	0.570 (0.018)	0.518 (0.016)	0.811 (0.011)	0.443 (0.010)	0.531 (0.013)	0.523 (0.020)	0.712 (0.005)	0.351 (0.015)
GraphDTA (2021)	0.565 (0.010)	0.527 (0.011)	0.763 (0.003)	0.399 (0.014)	0.501 (0.030)	0.531 (0.026)	0.665 (0.014)	0.241 (0.040)
ColdDTA (2023)	0.554 (0.008)	0.457 (0.012)	0.818 (0.024)	0.428 (0.020)	0.491 (0.018)	0.515 (0.030)	0.685 (0.027)	0.259 (0.012)
TransVAE-DTA (2024)	0.834 (0.034)	0.559 (0.012)	0.728 (0.017)	0.201 (0.022)	0.500 (0.038)	0.524 (0.047)	0.651 (0.038)	0.208 (0.022)
PairVAE (2025)	0.637 (0.010)	0.497 (0.009)	0.813 (0.006)	0.373 (0.050)	0.516 (0.033)	0.502 (0.005)	0.716 (0.014)	0.371 (0.025)
LaPro-DTA (ours)	0.519 (0.016)	0.449 (0.007)	0.828 (0.007)	0.473 (0.021)	0.489 (0.010)	0.491 (0.015)	0.726 (0.006)	0.403 (0.019)
<i>Setting: Unseen Pair</i>								
DeepDTA (2018)	0.886 (0.027)	0.737 (0.012)	0.712 (0.030)	0.072 (0.030)	0.708 (0.035)	0.590 (0.004)	0.631 (0.009)	0.166 (0.020)
AttentionDTA (2019)	0.837 (0.020)	0.696 (0.002)	0.715 (0.006)	0.114 (0.006)	0.674 (0.036)	0.564 (0.018)	0.631 (0.018)	0.165 (0.027)
Co-VAE (2021)	0.828 (0.026)	0.617 (0.025)	0.597 (0.011)	0.096 (0.005)	0.640 (0.005)	0.565 (0.019)	0.658 (0.006)	0.185 (0.002)
GraphDTA (2021)	0.874 (0.036)	0.606 (0.023)	0.631 (0.021)	0.032 (0.020)	0.643 (0.033)	0.573 (0.016)	0.597 (0.013)	0.055 (0.008)
ColdDTA (2023)	0.819 (0.012)	0.622 (0.008)	0.654 (0.014)	0.117 (0.013)	0.629 (0.010)	0.570 (0.016)	0.641 (0.008)	0.170 (0.014)
TransVAE-DTA (2024)	0.911 (0.039)	0.632 (0.013)	0.554 (0.020)	0.018 (0.012)	0.692 (0.018)	0.590 (0.038)	0.497 (0.003)	0.071 (0.033)
PairVAE (2025)	0.820 (0.032)	0.582 (0.001)	0.741 (0.010)	0.010 (0.003)	0.621 (0.020)	0.560 (0.006)	0.672 (0.009)	0.201 (0.012)
LaPro-DTA (ours)	0.727 (0.016)	0.546 (0.006)	0.770 (0.019)	0.166 (0.020)	0.637 (0.018)	0.558 (0.014)	0.660 (0.005)	0.194 (0.016)

Table 2: Performance comparison on Davis and KIBA datasets under cold-start scenarios. (Best, Second Best). Results are reported as mean (standard deviation) over five independent runs.

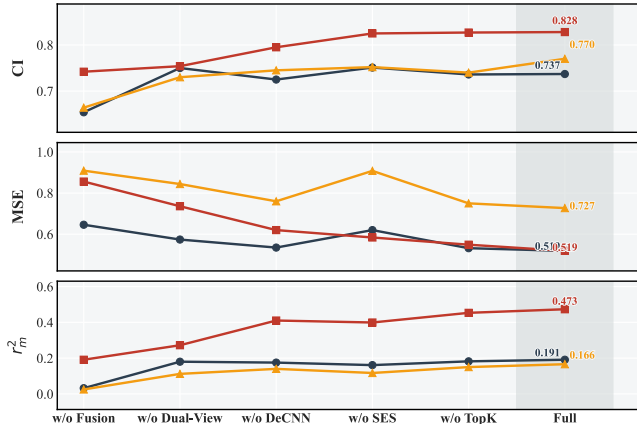


Figure 2: Ablation study on the Davis dataset.

Concordance Index (CI) measures the ranking consistency of the model. Additionally, r_m^2 [Pratim Roy *et al.*, 2009] is employed to assess the external predictive capability and reliability of the model on the test sets.

Baselines We benchmark LaPro-DTA against six representative state-of-the-art methods: DeepDTA [Öztürk *et al.*, 2018] employs dual CNNs for both drug and target encoding; AttentionDTA [Zhao *et al.*, 2019] integrates attention mechanisms with CNNs and BiRNNs; Co-VAE [Li *et al.*, 2021] applies a co-variational autoencoder for joint representation learning; GraphDTA [Nguyen *et al.*, 2021] processes drug molecular graphs using Graph Isomorphism Networks; TransVAE-DTA [Zhou *et al.*, 2024] combines transformers with VAEs

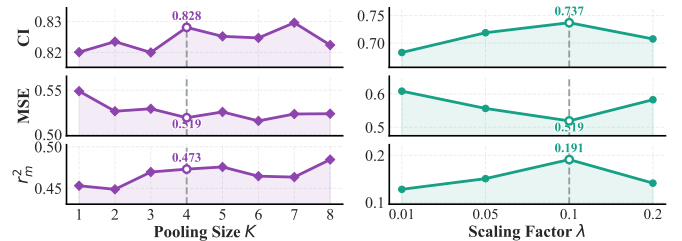


Figure 3: Parameter sensitivity analysis on the Davis dataset.

in a hybrid framework. Notably, ColdDTA [Fang *et al.*, 2023] performs data augmentation by randomly removing atomic groups from drug molecules to enhance generalization in cold-start scenarios. PairVAE [Qian *et al.*, 2025] utilizes multi-task learning combined with unsupervised strategies to improve model generalization. To ensure rigorous fairness, all baselines are **re-trained** on the experimental datasets, with hyperparameters referenced from the original literature and optimized on the specific experimental data.

3.3 Performance Comparison and Analysis

Table 2 reveals a universal performance decline across all the methods compared to random split benchmarks (details in Supplementary Materials), confirming the inherent difficulty of generalizing to unseen entities. Despite this challenge, LaPro-DTA consistently establishes new state-of-the-art results across most scenarios. In the *unseen drug* setting, the model demonstrates exceptional generalization, reducing MSE by 8.3% on Davis and 6.1% on KIBA relative to the

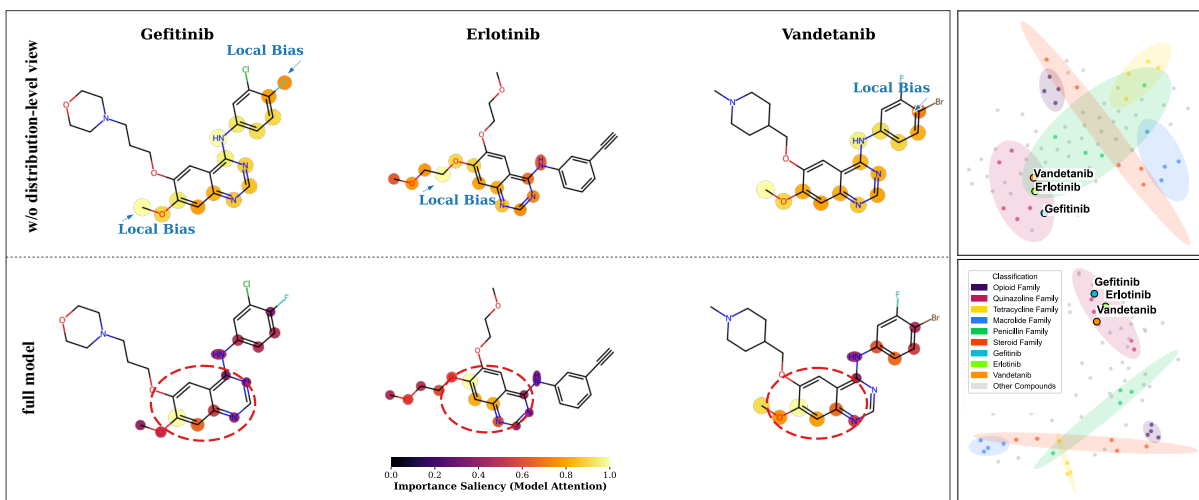


Figure 4: Saliency visualization of molecules with and without distribution-level view integration, and t-SNE projection of learned drug representations. The distinct clustering of drugs sharing similar scaffolds demonstrates that the model effectively captures discriminative structural semantics, mapping chemically similar compounds into proximal latent regions.

PDBbind ID	Year	Affinity (pK_d)	Pred. Affinity
5txy	2017	5.460	5.476804
6qlp	2019	5.280	5.301821
5u0e	2017	5.110	5.134590
6i12	2019	5.570	5.541025
6ma2	2018	5.389	5.419472
6ajv	2019	5.039	5.130577
⋮	⋮	⋮	⋮
Overall Performance (Mean MSE ↓)			
Pair-VAE			1.179
HiSIF-DTA (Top-Down)			0.978
LaPro-DTA (Ours)			0.855

Table 3: Predictive performance comparison on recent PDBbind entries (all methods evaluated under identical conditions).

strongest baselines. Similarly, in the *unseen target* scenario, it outperforms best methods by over 6.3% in terms of MSE on Davis. In the most rigorous *unseen pair* scenario, LaPro-DTA maintains competitive dominance. On the Davis dataset, it reduces MSE by 11.3% and improves *CI* by 3.9% compared to PairVAE. On the larger KIBA dataset, while PairVAE yields a marginally lower MSE, our method achieves a superior MAE. Notably, unlike PairVAE which relies on a computationally intensive generative framework, LaPro-DTA employs an efficient discriminative architecture. While PairVAE achieves marginally lower MSE on KIBA, our method strikes a superior balance between accuracy and complexity, demonstrating that mitigating overfitting alone enables robust extrapolation without the heavy computational cost of generative augmentation. These results demonstrate the strong generalization capability of the proposed method.

3.4 Ablation Study and Parameter Sensitivity

Effectiveness of Model Components. To validate the specific contribution of each module, we performed a comprehensive ablation study on the Davis dataset, as illustrated in Figure 2. First, replacing the cross-view multi-head attention

ID	Year	Structure	SMILES	True	Pred.	MSE	Avg.
5txy	2017		<chem>O=C1NC(=...2)O1</chem>	5.46	5.48	0.001	0.036
			<chem>O1C(=O)...ccc1</chem>	5.46	5.28	0.034	
			<chem>O=C1O[C@...ccc1</chem>	5.46	5.20	0.067	
			<chem>O=C1O[C@...N1</chem>	5.46	5.25	0.043	
6qlp	2019		<chem>Cc1ccc(...@H)2O</chem>	5.28	5.30	0.001	0.007
			<chem>Cc1ccc(...CO</chem>	5.28	5.26	0.001	
			<chem>Cc1ccc(...F)CO</chem>	5.28	5.19	0.008	
			<chem>Cc1ccc(...n1</chem>	5.28	5.14	0.019	
5u0e	2017		<chem>O=C1NC(...ccc1</chem>	5.11	5.13	0.001	0.036
			<chem>C([C@H...ccc1</chem>	5.11	5.42	0.096	
			<chem>c1cc(C[...c1</chem>	5.11	5.20	0.008	
			<chem>O=C1[C@...S</chem>	5.11	5.31	0.039	
6i12	2019		<chem>Cn1cc(N...3)cn1</chem>	5.57	5.54	0.001	0.004
			<chem>Cn1cc(N...0)cn1</chem>	5.57	5.60	0.001	
			<chem>Cn1cc(c...21)=O</chem>	5.57	5.65	0.007	
			<chem>Cn1ncc(...e3)c1</chem>	5.57	5.48	0.008	
6ma2	2018		<chem>COc1ccc...lccc1</chem>	5.39	5.42	0.001	0.028
			<chem>COc1c([...cc1</chem>	5.39	5.66	0.075	
			<chem>c1([C@H...c1</chem>	5.39	5.57	0.031	
			<chem>COc1ccc...H]2)=O</chem>	5.39	5.46	0.005	

Table 4: Robustness analysis on recent PDBbind entries (SMILES variants). SMILES strings are truncated, denoted by “...”.

mechanism with simple feature concatenation (w/o Fusion, standard in [Öztürk *et al.*, 2018; Li *et al.*, 2021]) results in the most severe degradation. This confirms that linear alignment fails to fully integrate the complex interactions between drug and target views. Second, removing the distribution-level view while retaining only the instance-level view (w/o Dual-View) sharply increases error in the unseen pair setting. This supports the hypothesis that the distribution-level view captures transferable chemical scaffolds essential for generalizing to novel entities. Meanwhile, replacing the structure-aware DeCNN module with an equivalent-parameter MLP (w/o DeCNN) degrades performance. This suggests that the inductive bias of convolution is better suited for preserving intrinsic molecular topology than flat projections. Finally, substituting pattern-aware top-*k* pooling with standard max pooling (w/o TopK, as in [Zhou *et al.*, 2024; Zhang *et al.*, 2024]) leads to a notable decline. This val-

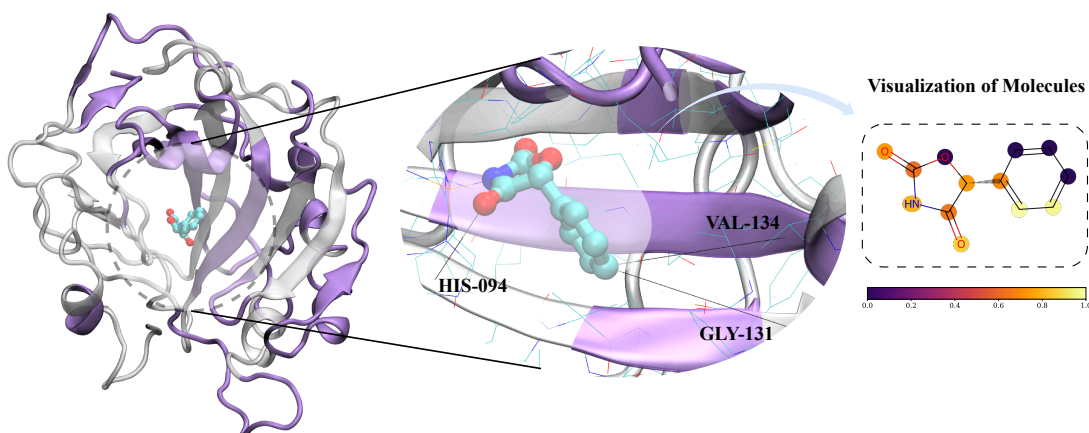


Figure 5: A saliency visualization of the drug–target binding pocket, where colored regions indicate key residues identified by the model.

indicates that top- k strategy effectively preserves critical bio-active residues and mitigates information loss caused by non-essential background sequences. These components function synergistically to secure optimal performance.

Parameter Sensitivity. We evaluate the impact of K and λ in Figure 3. Performance peaks at $K = 4$; larger values introduce background noise and cause **information loss**, validating the sparsity assumption of binding pockets. Similarly, $\lambda = 0.1$ yields the best results; lower values neglect global semantics while higher ones overwhelm instance’s local details, confirming 0.1 as the optimal balance for dual-view fusion.

3.5 Effectiveness of Distribution-Level View

To validate the capability of the distribution-level view in identifying drug scaffolds, we compared attention maps for structurally similar drugs, using Gefitinib as a case study (Figure 4). The baseline model relies solely on the instance-level view and exhibits structural myopia, causing it to overfit to spurious peripheral atoms. In contrast, the distribution-level view serves as a topological regularizer, redirecting focus toward the conserved main skeleton and key pharmacophores. This effect is further confirmed by t-SNE visualization [van der Maaten and Hinton, 2008], where related compounds show sharper clustering. These results demonstrate that the proposed synergy effectively corrects local biases by enforcing holistic structural constraints.

3.6 Robustness Analysis

Invariance to SMILES Permutations. To evaluate the generalization capability of LaPro-DTA, we selected recent entries from the PDBbind dataset (as shown in Table 4). Despite variations in SMILES linearization orders (generated by RDKit), LaPro-DTA exhibits remarkable stability. This observation indicates that the SES design effectively mitigates the model’s reliance on shortcuts inherent in SMILES syntax, enabling a clear decoupling between molecular semantics and syntactic permutations, and thereby preserving intrinsic molecular semantics.

3.7 Out-of-Sample Test

To rigorously evaluate generalization under a strict and impartial out-of-distribution setting, we adopt the external vali-

ation protocol from HiSIF-DTA [Bi *et al.*, 2023]. To fairly assess zero-shot transferability, all compared methods utilize models trained solely on the Davis dataset. These models are evaluated on 95 fresh PDBbind pairs that have zero overlap with the Davis dataset, ensuring no data leakage (see Supplementary Materials for details). As detailed in Table 3, LaPro-DTA achieves an MSE of **0.855**, significantly outperforming the HiSIF-DTA (12%) under identical conditions. These results confirm that our model effectively captures transferable physicochemical semantics rather than dataset-specific biases, enabling robust generalization to realistic molecular distributions beyond standard benchmarks.

3.8 Interpretability of Protein Feature Extraction

Binding Interface Localization. Figure 5 illustrates the interaction for the representative complex PDB 5txy. We conducted this visualization analysis using the Grad-CAM technique [Selvaraju *et al.*, 2017] and VMD software [Humphrey *et al.*, 1996]. The pattern-aware top- k Pooling effectively filters non-essential protein regions, concentrating high attention scores strictly around the actual binding pocket. Notably, critical contacting residues—including HIS-094, GLY-131, and VAL-134—are identified. This spatial alignment confirms that LaPro-DTA prioritizes physical interaction interfaces over irrelevant background sequences.

4 Conclusion

In this paper, we proposed LaPro-DTA to tackle the critical generalization bottleneck in cold-start DTA prediction. It effectively mitigates overfitting through a latent dual-view drug representation mechanism and alleviates information loss via a pattern-aware salient target feature extraction strategy. Extensive experiments demonstrate that LaPro-DTA not only establishes new state-of-art performance in challenging unseen settings but also offers interpretability into the underlying binding mechanisms. For future work, we plan to extend our framework beyond 1D sequences by integrating explicit geometric graphs or 3D conformers, aiming to unlock richer spatial dependencies for even more robust drug discovery.

A Related Works

Overview. Contemporary computational frameworks for DTA prediction generally comprise three core components: drug representation learning, target representation learning, and feature fusion. To articulate the motivation underlying LaPro-DTA, we systematically review the literature through the lens of this taxonomy.

A.1 Drug Representation Modeling

Pioneering studies, such as DeepDTA [Öztürk *et al.*, 2018] and WideDTA [Öztürk *et al.*, 2019], conceptualize SMILES strings as one-dimensional sequences, employing Convolutional Neural Networks (CNNs) or Recurrent Neural Networks (RNNs) to extract local patterns. Despite their efficacy, these sequence-based methods are prone to overfitting local lexical features, often failing to capture the intrinsic spatial geometry of molecules. To mitigate this limitation, GraphDTA [Nguyen *et al.*, 2021] represents drug molecules as graphs, leveraging Graph Neural Networks (GNNs) to explicitly encode topological dependencies. Building on this paradigm, GDilatedDTA [Zhang *et al.*, 2024] synergizes 2D molecular graph features with 1D sequence features, utilizing a hybrid GNN-CNN architecture to capture complementary multimodal information. Alternatively, Co-VAE [Li *et al.*, 2021] introduces a multi-task learning framework based on Variational Autoencoders (VAEs); by incorporating molecular reconstruction as an auxiliary objective, it facilitates the learning of regularized and semantic-rich latent drug representations.

A.2 Target Representation Modeling

Target representation modeling poses a more formidable challenge than drug encoding, primarily attributable to the extensive length and high information density of amino acid sequences. To capture local sequential motifs, Convolutional and Recurrent Neural Networks are widely adopted, as exemplified by DeepDTA [Öztürk *et al.*, 2018], WideDTA [Öztürk *et al.*, 2019], and AttentionDTA [Zhao *et al.*, 2019]. Advancing beyond standard architectures, Co-VAE [Li *et al.*, 2021] adapts the VAE framework to distill compact latent representations, whereas TransVAE-DTA [Zhou *et al.*, 2024] leverages Transformer encoders to model long-range dependencies and global context. Crucially, despite these advances in feature extraction, the prevailing paradigm relies disproportionately on rudimentary global pooling (*e.g.*, max or average pooling) to compress variable-length sequences into fixed-size vectors.

A.3 Feature Fusion Module

The feature fusion module serves as the nexus for synthesizing drug and target representations to predict binding affinity. Seminal models like DeepDTA [Öztürk *et al.*, 2018] relied on the rudimentary concatenation of global embeddings, a strategy that inevitably neglects fine-grained intermolecular interactions. To capture substructure-level dependencies, MolTrans [Huang *et al.*, 2021] constructs pairwise interaction maps between drug substructures and protein fragments,

explicitly modeling high-order interaction patterns. Subsequently, attention-driven paradigms further advanced interaction modeling: AttentionDTA [Zhao *et al.*, 2019] employs cross-attention mechanisms to isolate relevant interaction regions, whereas TransVAE-DTA [Zhou *et al.*, 2024] leverages Attention-based Pooling (AAP) for more discriminative feature aggregation. However, owing to severe compression of target features in upstream encoding, these attention mechanisms are prone to degeneration, significantly undermining their efficacy in capturing fine-grained bioactivity.

Despite the success achieved by existing methods, significant limitations persist. Specifically, drug and protein encoders typically rely on single-view embeddings, often overlooking explicit distribution perspectives for drugs and key local fragment information for proteins. Moreover, fusion modules—whether based on concatenation, interaction maps, or attention—generally lack mechanisms to enhance robustness or align complementary features. Consequently, these deficiencies severely limit the generalization capabilities of current models when encountering unseen drugs or targets.

B Supplementary Experiments

B.1 More Implementation Details

The detailed hyperparameter configurations are summarized in Table 5. We implemented LaPro-DTA using the PyTorch 2.0 framework on an NVIDIA GeForce RTX 3090 GPU. To prevent information leakage and simulate realistic cold-start scenarios, we applied a structured data splitting protocol (Algorithm 1). Let \mathcal{D} and \mathcal{P} denote the sets of drugs and proteins, respectively. We randomly partitioned these sets into disjoint subsets: $\mathcal{D} = \mathcal{D}_{seen} \cup \mathcal{D}_{unseen}$ and $\mathcal{P} = \mathcal{P}_{seen} \cup \mathcal{P}_{unseen}$.

Datasets. We evaluate LaPro-DTA on two standard benchmarks, **Davis** [Davis *et al.*, 2011] and **KIBA** [Tang *et al.*, 2014], while incorporating **BindingDB** [Liu *et al.*, 2007] to assess large-scale generalization. Davis contains 30,056 interactions (pK_d) between 68 drugs and 442 targets, whereas KIBA comprises 118,254 entries (KIBA scores) across 2,111 drugs and 229 targets. BindingDB serves as a supplementary testbed with broader chemical diversity.

B.2 Experiments on Random-Split Setting

Supplementary Baselines. To comprehensively validate the effectiveness of LaPro-DTA across different evaluation scenarios, we supplement our analysis by comparing it against a broader range of methods under the standard random split setting. The performance results for the following baselines are directly cited from their respective original publications:

- **KronRLS** [Nascimento *et al.*, 2016] and **SimBoost** [He *et al.*, 2017] serve as representative traditional machine learning baselines. KronRLS computes structural and sequence similarity kernels and employs Kronecker regularized least squares for prediction. SimBoost utilizes gradient boosting machines combined with feature engineering to model drug-target pairs.
- **DeepDTA** [Öztürk *et al.*, 2018] is a pioneering deep learning framework that treats drug SMILES and protein amino acid sequences as 1D text data, employing

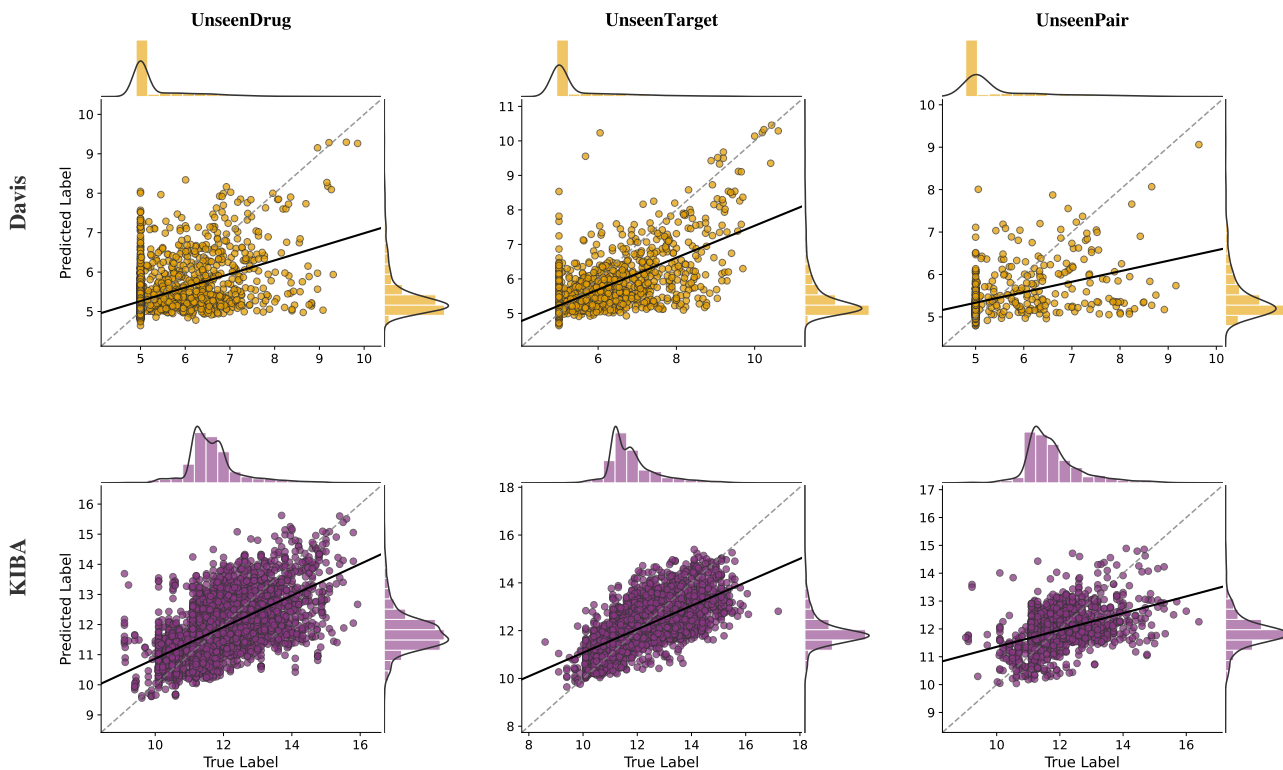


Figure 6: True affinity value against the predicted value on Davis and KIBA datasets.

dual Convolutional Neural Networks (CNNs) to extract local latent patterns.

- **WideDTA** [Öztürk *et al.*, 2019] improves upon DeepDTA by adopting a "word-based" approach. Instead of character-level inputs, it utilizes Ligand Maximum Common Substructures (LMCS) and protein motifs as input words for CNNs to capture higher-level semantic features.
- **AttentionDTA** [Zhao *et al.*, 2019] incorporates attention mechanisms into the sequence modeling process. By weighting the interaction intensity between drug and protein subsequences, it aims to focus the model on the most relevant binding regions.
- **GraphDTA** [Nguyen *et al.*, 2021] represents a significant shift towards geometric deep learning. It models drug molecules as 2D graphs and investigates various Graph Neural Networks (including GCN, GAT, and GIN) to explicitly capture the topological dependencies of atoms, achieving strong baseline performance.
- **DeepCDA** [Abbasi *et al.*, 2020] combines CNNs with Long Short-Term Memory (LSTM) networks. It is designed to capture both local features and long-term sequential dependencies, emphasizing effective encoding for cross-domain affinity prediction.
- **Co-VAE** [Li *et al.*, 2021] employs a multi-task learning strategy based on Variational Autoencoders (VAEs). It generates latent representations by jointly optimizing for

affinity prediction and the reconstruction of molecular sequences.

- **DoubleSG-DTA** [Qian *et al.*, 2023] introduces a multi-view fusion strategy. It extracts features from both the SMILES sequence (via CNN) and the molecular graph (via GNN), integrating these dual representations to enhance drug encoding.
- **GDilatedDTA** [Zhang *et al.*, 2024] addresses the issue of long-range dependencies and signal loss. It utilizes dilated graph convolutions for drugs and dilated 1D convolutions for proteins to expand the receptive field without increasing model complexity.

Table 6 reports the performance of LaPro-DTA against representative baselines under the random-split setting, following the protocol of [Zhang *et al.*, 2024]. Collectively, these experimental results validate the superiority of our proposed method across multiple benchmark datasets.

Comparative Results and Analysis

The empirical results presented in Table 6 demonstrate that LaPro-DTA establishes new state-of-the-art (SOTA) performance across the majority of evaluation scenarios.

On the KIBA dataset, our model achieves an optimal MSE of 0.133 and a CI of 0.891. Notably, this performance significantly surpasses not only the 1D-based DeepDTA but also the 2D graph-based GraphDTA (which yields an MSE of 0.147). This substantial margin confirms that our proposed Gated 1D

Algorithm 1: Cold-Start Data Splitting Algorithm

Input: Interaction Matrix \mathbf{A} , Unseen Ratio ρ
Output: Train Set \mathcal{D}_{train} , Val Set \mathcal{D}_{val} , Test Sets $\{\mathcal{D}_{S2}, \mathcal{D}_{S3}, \mathcal{D}_{S4}\}$

```
/* Step 1: Entity-Level Partitioning */
Set random seed  $s$ ;
Identify active drugs  $\mathcal{I}_d$  and proteins  $\mathcal{I}_p$  from  $\mathbf{A}$ ;
 $K_d \leftarrow \lfloor \rho \times |\mathcal{I}_d| \rfloor, K_p \leftarrow \lfloor \rho \times |\mathcal{I}_p| \rfloor$ ;
Randomly select unseen sets  $\mathcal{U}_d \subset \mathcal{I}_d, \mathcal{U}_p \subset \mathcal{I}_p$  of size  $K_d, K_p$ ;
Define seen sets  $\mathcal{S}_d \leftarrow \mathcal{I}_d \setminus \mathcal{U}_d, \mathcal{S}_p \leftarrow \mathcal{I}_p \setminus \mathcal{U}_p$ ;
/* Step 2: Interaction Allocation */
Initialize  $\mathcal{D}_{train}, \mathcal{D}_{val}, \mathcal{D}_{S2}, \mathcal{D}_{S3}, \mathcal{D}_{S4} \leftarrow \emptyset$ ;
for each interaction  $(d, p)$  such that  $\mathbf{A}_{d,p} > 0$  do
  if  $d \in \mathcal{S}_d$  and  $p \in \mathcal{S}_p$  then
    // Seen Drug, Seen Protein
    Add  $(d, p)$  to  $\mathcal{D}_{train}$ ;
  else
    Generate random  $r \sim Uniform(0, 1)$ ;
    if  $d \in \mathcal{U}_d$  and  $p \in \mathcal{S}_p$  then
      // New Drug (S2)
      if  $r < 0.5$  then Add to  $\mathcal{D}_{val}$ ;
      else Add to  $\mathcal{D}_{S2}$ ;
    else if  $d \in \mathcal{S}_d$  and  $p \in \mathcal{U}_p$  then
      // New Protein (S3)
      if  $r < 0.5$  then Add to  $\mathcal{D}_{val}$ ;
      else Add to  $\mathcal{D}_{S3}$ ;
    else if  $d \in \mathcal{U}_d$  and  $p \in \mathcal{U}_p$  then
      // Both New (S4)
      if  $r < 0.5$  then Add to  $\mathcal{D}_{val}$ ;
      else Add to  $\mathcal{D}_{S4}$ ;
    end
  end
end
return  $\mathcal{D}_{train}, \mathcal{D}_{val}, \mathcal{D}_{S2}, \mathcal{D}_{S3}, \mathcal{D}_{S4}$ ;
```

representation is highly effective, capturing critical local biochemical features that conventional CNNs or graph convolutions may overlook.

Regarding the Davis dataset, LaPro-DTA yields the best ranking performance with a CI of 0.895 and the highest prediction stability with an r_m^2 of 0.693. Although AttentionDTA exhibits a marginal lead in MSE, our model demonstrates superior capability in correctly ranking drug-target pairs (indicated by CI) and maintaining predictive consistency (indicated by r_m^2). This suggests that LaPro-DTA is less biased towards the distribution mean and more robust in distinguishing relative affinity differences. Furthermore, on the BindingDB dataset, which represents a much larger and more heterogeneous chemical space, LaPro-DTA consistently secures the top position in both MSE and CI. This evidence strongly supports the robustness of our framework, proving that the synergy of dual-view drug modeling and pattern-aware target pooling enables superior generalization across

Table 5: Hyperparameter settings of LaPro-DTA.

Hyperparameter	Value
Drug Representation	
Embedding Dimension	128
CNN Filter Sizes	[4, 4, 4]
Number of Filters	128
DeconvNet Layers	3
Latent Dimension (z)	96
Target Representation	
Embedding Dimension	128
CNN Filter Sizes	[4, 8, 12]
Top- K Pooling Size (K)	4
Number of CNN Layers	3
Interaction Module	
Attention Heads	4
Attention Hidden Dim (d_k)	96
MLP Hidden Units	[1024, 512]
Optimization	
Optimizer	Adam
Learning Rate	5×10^{-4}
Batch Size (KIBA / Davis)	256 / 32
Max Epochs (Cold / Rand)	100 / 500
Dropout Rate	0.1
Weight Decay	1×10^{-4}

diverse molecular scaffolds and protein families.

Despite these challenges, LaPro-DTA demonstrates superior predictive capabilities. On the Davis dataset, our model achieves a substantial reduction in prediction error (MSE) compared to the strongest baseline, TransVAE-DTA, while establishing a new benchmark for ranking accuracy (CI). Although the predictive stability metric (r_m^2) remains comparable to the leading method, the distinct advantage in precision highlights the effectiveness of our feature fusion strategy.

On the larger KIBA dataset, the performance gap is even more pronounced. LaPro-DTA achieves comprehensive dominance, consistently outperforming previous state-of-the-art methods across all metrics. This indicates that the proposed dual-view mechanism and pattern-aware pooling not only enhance generalization in cold-start scenarios but also effectively refine feature granularity for standard interaction prediction tasks.

B.3 Ablation Study and Parameter Sensitivity

Ablation Study. As detailed in the main text, Table 7 presents the comprehensive ablation results under three cold-start settings. The results consistently indicate that removing any specific module—whether the latent dual-view mechanism, top- k pooling, or cross-view fusion—leads to performance degradation across all evaluation metrics. This confirms that the complete framework is essential for achieving robust generalization when extrapolating to unseen biochemical entities.

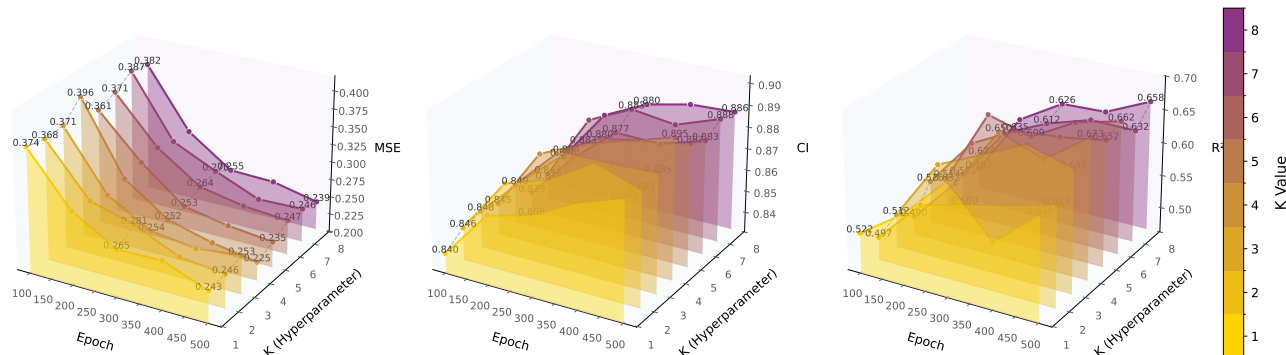
To further verify the contribution of each module in stan-

Table 6: Performance comparison of representative DTA models on KIBA, Davis, and BindingDB datasets. (**Best**, Second Best).

Model	KIBA Dataset			Davis Dataset			BindingDB Dataset		
	MSE↓	CI↑	r_m^2 ↑	MSE↓	CI↑	r_m^2 ↑	MSE↓	CI↑	r_m^2 ↑
KronRLS (2015)	0.411	0.782	0.342	0.379	0.871	0.407	0.910	0.710	–
SimBoost (2017)	0.222	0.836	0.629	0.282	0.872	0.644	–	–	–
DeepDTA (2018)	0.194	0.863	0.630	0.261	0.878	0.630	0.633	0.844	0.633
WideDTA (2019)	0.179	0.875	–	0.262	0.886	–	–	–	–
AttentionDTA (2022)	0.155	0.882	0.755	0.216	0.887	0.677	0.745	0.542	–
GraphDTA (GIN) (2021)	<u>0.147</u>	0.891	0.687	0.229	<u>0.893</u>	0.663	0.535	0.858	–
DeepCDA (2020)	0.176	0.889	0.682	0.248	0.891	0.649	0.848	0.722	0.531
Co-VAE (New-drug) (2022)	0.416	0.742	0.358	0.724	0.712	0.107	–	–	–
Co-VAE (New-target) (2022)	0.421	0.741	0.356	0.419	0.816	0.477	–	–	–
DoubleSG-DTA (2023)	0.164	0.856	0.721	0.250	0.886	<u>0.688</u>	0.533	0.862	<u>0.726</u>
GDilatedDTA (2024)	0.156	0.876	0.775	0.237	0.885	0.686	<u>0.483</u>	<u>0.868</u>	0.730
LaPro-DTA (Ours)	0.133	0.891	<u>0.760</u>	<u>0.225</u>	0.895	0.693	0.466	0.874	0.706

Table 7: Ablation study of LaPro-DTA on the Davis dataset under three cold-start settings. **Dual**: Latent Dual-View Mechanism; **TopK**: top- k Pooling; **Fusion**: Cross-View Attention. The best results are highlighted in **bold**, and the second-best results are underlined. “↑” indicates higher is better, “↓” indicates lower is better.

Components			Unseen Drug			Unseen Target			Unseen Pair		
Dual	TopK	Fusion	CI (↑)	MSE (↓)	r_m^2 (↑)	CI (↑)	MSE (↓)	r_m^2 (↑)	CI (↑)	MSE (↓)	r_m^2 (↑)
–	–	–	0.723	0.567	0.137	<u>0.808</u>	0.654	0.368	0.728	0.836	0.104
✓	–	✓	<u>0.736</u>	<u>0.532</u>	0.181	0.798	<u>0.548</u>	<u>0.453</u>	<u>0.739</u>	<u>0.750</u>	<u>0.150</u>
–	✓	✓	0.726	0.542	0.201	0.755	0.752	0.302	<u>0.739</u>	0.804	0.124
✓	✓	–	0.654	0.646	0.032	0.742	0.856	0.191	0.664	0.909	0.025
✓	✓	✓	0.737	0.519	<u>0.191</u>	0.828	0.519	0.473	0.770	0.727	0.166

Figure 7: Comparison of MSE, CI and r_m^2 of LaPro-DTA with different K on the Davis dataset.

standard evaluation scenarios, we conducted an ablation study on the Davis dataset using random splitting, as summarized in Table 8. Comparing the baseline with the variant using only top- k pooling reveals a sharp reduction in prediction error (MSE). This suggests that the top- k strategy effectively filters out uninformative background noise in protein sequences, allowing the model to focus on high-confidence binding motifs

even when training and testing data share similar distributions. Similarly, the introduction of the feature fusion module significantly boosts the concordance index, highlighting the critical role of attention-based interaction modeling in correctly ranking the relative affinities of drug-target pairs. Ultimately, the integration of the latent dual-view mechanism with these components yields the best overall performance.

Table 8: Ablation study on the Davis dataset under the **random split** setting. **Dual**: latent dual-view (only instance-level view); **TopK**: top- k pooling; **Fusion**: cross-view attention.

Components			Metrics		
Dual	TopK	Fusion	CI (\uparrow)	MSE (\downarrow)	r_m^2 (\uparrow)
×	×	×	0.854	0.347	0.559
×	✓	×	0.875	0.240	<u>0.663</u>
×	×	✓	<u>0.885</u>	0.262	<u>0.598</u>
×	✓	✓	0.881	0.242	0.651
✓	×	✓	0.880	0.258	0.607
✓	✓	×	0.882	<u>0.239</u>	0.641
✓	✓	✓	0.895	0.225	0.693

The dual-view approach complements local feature extraction by enforcing global structural consistency, which proves particularly beneficial for improving predictive stability. These results confirm that the proposed modules fundamentally enhance representation and reasoning capabilities beyond just cold-start generalization.

Parameter Sensitivity. In addition to the cold-start experiments, we also conducted a sensitivity analysis on the key parameter K under the random split setting on the Davis dataset. As illustrated in Figure 7, as K increases from 1, the model performance exhibits a clear improvement in the early stage: MSE decreases substantially with increasing K , indicating reduced prediction error, while CI and r_m^2 consistently increase, reflecting simultaneous enhancements in ranking capability and goodness of fit. Notably, when $K > 1$, the model consistently outperforms the case of $K = 1$, demonstrating that the proposed top- k Pooling effectively strengthens the representation of drug fragment-level features. As K continues to increase, the variations of all three metrics gradually diminish, and the model performance converges to a stable regime without noticeable degradation.

B.4 Experimental Analysis

Scatter Plots of Prediction Performance. Figure 6 illustrates the scatter plots of predicted versus observed binding affinities on the Davis and KIBA datasets under three cold-start settings. As shown, the predictions of LaPro-DTA are tightly clustered around the identity line across all scenarios, indicating strong consistency between predicted and observed affinities. Notably, the model exhibits particularly strong performance in the unseen drug setting on the KIBA dataset, where the scatter points are most concentrated. In contrast, a higher degree of dispersion is observed in the unseen target setting, suggesting that this scenario remains more challenging for accurate affinity prediction.

References

[Abbasi *et al.*, 2020] Karim Abbasi, Parvin Razzaghi, Antti Poso, Massoud Amanlou, Jahan B Ghasemi, and Ali Masoudi-Nejad. DeepCDA: deep cross-domain compound-protein affinity prediction through lstm

and convolutional neural networks. *Bioinformatics*, 36(17):4633–4642, 2020.

[Ain *et al.*, 2015] Qurrat Ul Ain, Antoniya Aleksandrova, Florian D Roessler, and Pedro J Ballester. Machine-learning scoring functions to improve structure-based binding affinity prediction and virtual screening. *Wiley Interdisciplinary Reviews: Computational Molecular Science*, 5(6):405–424, 2015.

[Bemis and Murcko, 1996] Guy W Bemis and Mark A Murcko. The properties of known drugs. 1. Molecular frameworks. *Journal of Medicinal Chemistry*, 39(15):2887–2893, 1996.

[Bi *et al.*, 2023] Xiangpeng Bi, Shugang Zhang, Wenjian Ma, Huasen Jiang, and Zhiqiang Wei. HiSIF-DTA: a hierarchical semantic information fusion framework for drug-target affinity prediction. *IEEE Journal of Biomedical and Health Informatics*, 2023.

[Bishop, 1995] Chris M Bishop. Training with noise is equivalent to Tikhonov regularization. *Neural computation*, 7(1):108–116, 1995.

[Chen *et al.*, 2025] Shihong Chen, Haicheng Yi, Zhuhong You, Xuequn Shang, Yu-An Huang, Lei Wang, and Zhen Wang. Local-Global structure-aware geometric equivariant graph representation learning for predicting Protein-ligand binding affinity. *IEEE Transactions on Neural Networks and Learning Systems*, 2025.

[Choppara and Lokesh, 2025] Prashanth Choppara and Bommareddy Lokesh. Q-BAFNet: A hybrid quantum classical approach for drug-target binding affinity prediction. *IEEE Transactions on Computational Biology and Bioinformatics*, 2025.

[Dauphin *et al.*, 2017] Yann N Dauphin, Angela Fan, Michael Auli, and David Grangier. Language modeling with gated convolutional networks. In *International conference on machine learning*, pages 933–941. PMLR, 2017.

[Davis *et al.*, 2011] Mindy I Davis, Jeremy P Hunt, Sanna Herrgard, Pietro Cicceri, Lisa M Wodicka, Gabriel Pal-lares, Michael Hocker, Daniel K Treiber, and Patrick P Zarrinkar. Comprehensive analysis of kinase inhibitor selectivity. *Nature Biotechnology*, 29(11):1046–1051, 2011.

[Fang *et al.*, 2023] Kejie Fang, Yiming Zhang, Shiyu Du, and Jian He. ColdDTA: utilizing data augmentation and attention-based feature fusion for drug-target binding affinity prediction. *Computers in Biology and Medicine*, 164:107372, 2023.

[He *et al.*, 2017] Tong He, Marten Heidemeyer, Fuqiang Ban, Artem Cherkasov, and Martin Ester. SimBoost: a read-across approach for predicting drug-target binding affinities using gradient boosting machines. *Journal of cheminformatics*, 9(1):24, 2017.

[He *et al.*, 2025] Haohuai He, Guanxing Chen, Zhenchao Tang, and Calvin Yu-Chian Chen. Dual modality feature fused neural network integrating binding site information for drug target affinity prediction. *NPJ Digital Medicine*, 8(1):67, 2025.

- [Huang *et al.*, 2021] Kexin Huang, Cao Xiao, Lucas M Glass, and Jimeng Sun. MolTrans: molecular interaction transformer for drug–target interaction prediction. *Bioinformatics*, 37(6):830–836, 2021.
- [Huang *et al.*, 2025] Zibo Huang, Xinrui Weng, and Le Ouyang. GFLearn: Generalized feature learning for drug-target binding affinity prediction. *IEEE Journal of Biomedical and Health Informatics*, 2025.
- [Humphrey *et al.*, 1996] William Humphrey, Andrew Dalke, and Klaus Schulten. VMD: visual molecular dynamics. *Journal of molecular graphics*, 14(1):33–38, 1996.
- [Kalchbrenner *et al.*, 2014] Nal Kalchbrenner, Edward Grefenstette, and Phil Blunsom. A convolutional neural network for modelling sentences. In *Proceedings of the 52nd Annual Meeting of the Association for Computational Linguistics (ACL)*, pages 655–665, 2014.
- [Kim *et al.*, 2021] QHwan Kim, Joon-Hyuk Ko, Sunghoon Kim, Nojun Park, and Wonho Jhe. Bayesian neural network with pretrained protein embedding enhances prediction accuracy of drug-protein interaction. *Bioinformatics*, 37(20):3428–3435, 2021.
- [Li *et al.*, 2020] Shuya Li, Fangping Wan, Hantao Shu, Tao Jiang, Dan Zhao, and Jianyang Zeng. MONN: A multi-objective neural network for predicting pairwise non-covalent interactions and binding affinities between compounds and proteins. In *International Conference on Research in Computational Molecular Biology*, pages 259–260. Springer, 2020.
- [Li *et al.*, 2021] Tianjiao Li, Xing-Ming Zhao, and Limin Li. Co-VAE: Drug-target binding affinity prediction by co-regularized variational autoencoders. *IEEE Transactions on Pattern Analysis and Machine Intelligence*, 44(12):8861–8873, 2021.
- [Li *et al.*, 2023] Mei Li, Ye Cao, Xiaoguang Liu, and Hua Ji. Structure-aware graph attention diffusion network for protein–ligand binding affinity prediction. *IEEE Transactions on Neural Networks and Learning Systems*, 2023.
- [Liu *et al.*, 2007] Tiqing Liu, Yuhmei Lin, Xin Wen, Robert N Jorissen, and Michael K Gilson. BindingDB: a web-accessible database of experimentally determined protein–ligand binding affinities. *Nucleic acids research*, 35(suppl_1):D198–D201, 2007.
- [Nascimento *et al.*, 2016] André CA Nascimento, Ricardo BC Prudêncio, and Ivan G Costa. A multiple kernel learning algorithm for drug-target interaction prediction. *BMC Bioinformatics*, 17(1):46, 2016.
- [Nguyen *et al.*, 2021] Thin Nguyen, Hang Le, Thomas P Quinn, Tri Nguyen, Thuc Duy Le, and Svetha Venkatesh. GraphDTA: predicting drug–target binding affinity with graph neural networks. *Bioinformatics*, 37(8):1140–1147, 2021.
- [Öztürk *et al.*, 2018] Hakime Öztürk, Arzucan Özgür, and Elif Ozkirimli. DeepDTA: deep drug–target binding affinity prediction. *Bioinformatics*, 34(17):i821–i829, 2018.
- [Öztürk *et al.*, 2019] Hakime Öztürk, Elif Ozkirimli, and Arzucan Özgür. WideDTA: prediction of drug-target binding affinity. *arXiv preprint arXiv:1902.04166*, 2019.
- [Prasad and Mailankody, 2017] Vinay Prasad and Sham Mailankody. Research and development spending to bring a single cancer drug to market and revenues after approval. *JAMA internal medicine*, 177(11):1569–1575, 2017.
- [Pratim Roy *et al.*, 2009] Partha Pratim Roy, Somnath Paul, Indrani Mitra, and Kunal Roy. On two novel parameters for validation of predictive QSAR models. *Molecules*, 14(5):1660–1701, 2009.
- [Qian *et al.*, 2023] Yongtao Qian, Wanxing Ni, Xingxing Xianyu, Liang Tao, and Qin Wang. DoubleSG-DTA: deep learning for drug discovery: case study on the non-small cell lung cancer with EGFR T 790 M mutation. *Pharmaceutics*, 15(2):675, 2023.
- [Qian *et al.*, 2025] Yining Qian, Xuewen Zhang, and An-Yang Lu. Pair-vae: Variational pairwise augmentation with label sharing for generalizable drug-target interaction prediction. In *2025 IEEE International Conference on Bioinformatics and Biomedicine (BIBM)*, pages 693–698. IEEE, 2025.
- [Selvaraju *et al.*, 2017] Ramprasaath R Selvaraju, Michael Cogswell, Abhishek Das, Ramakrishna Vedantam, Devi Parikh, and Dhruv Batra. Grad-CAM: Visual explanations from deep networks via gradient-based localization. In *Proceedings of the IEEE international conference on computer vision*, pages 618–626, 2017.
- [Shah *et al.*, 2025] Pir Masoom Shah, Huimin Zhu, Zhangli Lu, Kaili Wang, Jing Tang, and Min Li. DeepDTAGen: a multitask deep learning framework for drug-target affinity prediction and target-aware drugs generation. *Nature Communications*, 16(1):5021, 2025.
- [Tang *et al.*, 2014] Jing Tang, Agnieszka Szwajda, Sushil Shakyawar, Tao Xu, Petteri Hintsanen, Krister Wennerberg, and Tero Aittokallio. Making sense of large-scale kinase inhibitor bioactivity data sets: a comparative and integrative analysis. *Journal of chemical information and modeling*, 54(3):735–743, 2014.
- [van der Maaten and Hinton, 2008] Laurens van der Maaten and Geoffrey Hinton. Visualizing data using t-sne. *Journal of Machine Learning Research*, 9(11):2579–2605, 2008.
- [Watanabe *et al.*, 2021] Narumi Watanabe, Yuuto Ohnuki, and Yasubumi Sakakibara. Deep learning integration of molecular and interactome data for protein–compound interaction prediction. *Journal of Cheminformatics*, 13(1):36, 2021.
- [Weininger, 1988] David Weininger. SMILES, a chemical language and information system. 1. introduction to methodology and encoding rules. *Journal of chemical information and computer sciences*, 28(1):31–36, 1988.
- [Yang *et al.*, 2024] Ziduo Yang, Weihe Zhong, Qiujie Lv, Tiejun Dong, Guanxing Chen, and Calvin Yu-Chian Chen. Interaction-based inductive bias in graph neural networks: enhancing protein-ligand binding affinity predictions from

- 3D structures. *IEEE Transactions on Pattern Analysis and Machine Intelligence*, 46(12):8191–8208, 2024.
- [Zeiler *et al.*, 2010] Matthew D Zeiler, Dilip Krishnan, Graham W Taylor, and Rob Fergus. Deconvolutional networks. In *2010 IEEE Computer Society Conference on computer vision and pattern recognition*, pages 2528–2535. IEEE, 2010.
- [Zhang *et al.*, 2024] Longxin Zhang, Wenliang Zeng, Jingsheng Chen, Jianguo Chen, and Keqin Li. GDilatedDTA: Graph dilation convolution strategy for drug target binding affinity prediction. *Biomedical Signal Processing and Control*, 92:106110, 2024.
- [Zhao *et al.*, 2019] Qichang Zhao, Fen Xiao, Mengyun Yang, Yaohang Li, and Jianxin Wang. AttentionDTA: prediction of drug–target binding affinity using attention model. In *2019 IEEE International Conference on Bioinformatics and Biomedicine (BIBM)*, pages 64–69. IEEE, 2019.
- [Zhao *et al.*, 2020] Lingling Zhao, Junjie Wang, Long Pang, Yang Liu, and Jun Zhang. GANsDTA: Predicting drug-target binding affinity using GANs. *Frontiers in genetics*, 10:1243, 2020.
- [Zhou *et al.*, 2024] Changjian Zhou, Zhongzheng Li, Jia Song, and Wensheng Xiang. TransVAE-DTA: Transformer and variational autoencoder network for drug-target binding affinity prediction. *Computer Methods and Programs in Biomedicine*, 244:108003, 2024.